




Article

Tunable Multi-Band-Stop Filters Using Generalized Fibonacci Photonic Crystals for Optical Communication Applications

Naim Ben Ali ^{1,2,*} , Serhan Alshammari ¹ , Youssef Trabelsi ^{2,3}, Haitham Alsaif ⁴ , Omar Kahouli ⁵ and Zied Elleuch ⁶

¹ Department of Industrial Engineering, College of Engineering, University of Ha'il, Ha'il 2440, Saudi Arabia; s.alshammari@uoh.edu.sa

² Photovoltaic and Semiconductor Materials Laboratory, National Engineering School of Tunis, University of Tunis El Manar, Tunis 1002, Tunisia; ytrabelsi@kku.edu.sa

³ Physics Department, College of Arts and Sciences in Muhail Asir, King Khalid University, Abha 61421, Saudi Arabia

⁴ Department of Electrical Engineering, College of Engineering, University of Ha'il, Ha'il 2440, Saudi Arabia; h.alsaif@uoh.edu.sa

⁵ Department of Electronics Engineering, Applied College, University of Ha'il, Ha'il 2440, Saudi Arabia; a.kahouli@uoh.edu.sa

⁶ Department of Computer Science, Applied College, University of Ha'il, Ha'il 2440, Saudi Arabia; zi.elleuch@uoh.edu.sa

* Correspondence: na.benali@uoh.edu.sa or naimgi2@yahoo.fr; Tel.: +966-595569515

Abstract: In this study, a numerical investigation of photonic quasi-periodic Generalized Fibonacci (GF) (m, n) sequences is carried out in the visible spectrum. The transfer matrix method is employed to study the behavior of wave propagation through the photonic structures. Firstly and to highlight the importance of the GF structure, its transmittance spectrum is compared to those of periodic and ordinary Fibonacci structures. It is shown that the GF structure permits one to obtain multi-photonic band gaps (PBGs) separated by several resonance modes. The variation in the parameter m of the GF $(m, 1)$ structure allows for the tuning of the number, the position and the width of these bands. By changing the parameter m , the wavelengths (650, 850, 1300, and 1550 nm) of the plastic and glass optical fibers can be allowed or forbidden to transmit through the structure according to the value of this parameter. In contrast, the variation in the parameter n for GF $(1, n)$ hides all PBGs and only permits the appearance of several Kiessig fringes. The proposed structures can find application as tunable multi-band-stop filters for optical fiber wavelengths.

Keywords: generalized Fibonacci sequences; photonic; transfer matrix method; band-stop filters; optical communication; photonic band gap

MSC: 37M10



Citation: Ali, N.B.; Alshammari, S.; Trabelsi, Y.; Alsaif, H.; Kahouli, O.; Elleuch, Z. Tunable Multi-Band-Stop Filters Using Generalized Fibonacci Photonic Crystals for Optical Communication Applications. *Mathematics* **2022**, *10*, 1240. <https://doi.org/10.3390/math10081240>

Academic Editor: Nikolaos Tsitsas

Received: 21 February 2022

Accepted: 7 April 2022

Published: 9 April 2022

Publisher's Note: MDPI stays neutral with regard to jurisdictional claims in published maps and institutional affiliations.



Copyright: © 2022 by the authors. Licensee MDPI, Basel, Switzerland. This article is an open access article distributed under the terms and conditions of the Creative Commons Attribution (CC BY) license (<https://creativecommons.org/licenses/by/4.0/>).

1. Introduction

An ordinary periodic photonic structure can be designed by iterating a finite unit cell several times, and each cell is composed of two or more different layers of materials. However, a random structure follows no particular rule, and the distribution of layers is chaotic. Quasi-periodic structures present another category of structures, and they are neither periodic nor random but a sequence that is located between these two sequences [1]. These quasi-periodic structures are made up of two or more different layers with different materials, and they follow a well-determined mathematical distribution [2,3]. Their impressive property in transmission spectra permits the continuity of the existing central forbidden gaps (PBGs) in periodic photonic structures with strong resonance modes to be broken. These modes localize light very effectively [2–7]. The most well-studied and well-known quasi-periodic sequences are the Fibonacci sequence (FS) [3,5,8–10], the Thue–Morse

sequence (TMS) [3,4,11] and the Cantor sequence (CS) [3,12,13]. These quasi-periodic structures find application in several optical, infrared, and microwave fields. They are proposed as structures that allow light to be slowed down and localized [3,4,14], which paves the way toward the realization of optical microprocessors [15], optical connectors [16], optical memories [17,18], and quantum computers [19,20]. In addition, these quasi-periodic structures [3,21,22] are used as filters [5,6,8,23,24] and high omnidirectional reflectors [25–31] in optical communication devices. These filters permit undesirable frequencies or noises to be discarded. In addition, omnidirectional reflectors are used to construct micro-cavity lasers and photonic quantum computers (as a substrate of the antennas to improve their directivity [32]) and to improve the gain for THz photoconductive antennas [33]. The localization of light makes it possible to enhance the interaction between the photon and matter, which then makes it possible to slow down the group velocity of light [3]. This property paves the way toward the construction of optical memories [34,35] and photonic quantum computers [36]. Optical memories will then use photons instead of electrons in ordinary memory. In addition, optical memories will then have a huge capacity to store information. To develop a photonic quantum computer, recently, Ben Bartlett et al. [36] experimented with a new device composed of a photonic cavity, waveguides, an optical fiber storage ring, and optical switches. This device permits the development of a quantum information processor, where optical qubits have very long coherence times, are maintainable at room temperature, and are optimal for quantum communication. In addition to all of the above applications, the resonance modes provided by quasi-periodic photonic structures make it possible to design new sensors, for example, for biomedical sensing [37], for water quality control [38], and for humidity sensing [39]. In addition to solid materials permitting the control of light, liquid materials can take the same role. For example, Lio, G.E. et al. [40] proposed an optical beam steering device operating at a wavelength of 1550 nm and based on a high index material such as molybdenum disulfide (MoS₂), where the direction of light is actively controlled by means of a liquid crystal. This dynamic beam steering for light detection and ranging (LIDAR) applications can be achieved by controlling the amplitude, losses, and deflection of light with elements of an optical array [40]. In addition, Shaltout, A.M. et al. [41] proposed ultrathin optical cavities with embedded photonic metasurfaces, which permit high spatial resolution color filtering and spectral imaging to be obtained. These optical cavities find application in compact integrated optical systems on a chip, such as high-resolution spatial light modulators, VCSELs, bio-sensors, and imaging spectroscopy systems. Furthermore, Giuseppe, E.L. et al. [42] proposed plasmonic metal–insulator nanocavities that can be exploited as tunable color filters, photonics, optical sensors, and physical security agents. The resonant wavelengths of these nanocavities have extraordinary transmission with zero reflection for different incident polarizations. In the field of frequency-selective filters, previous studies can be presented. For example, S. Tibuleac et al. [43] used dielectric waveguide gratings and, by embedding the gratings in layered antireflection structures, proposed a frequency-selective structure based on guided-mode resonance effects. The proposed filters were built and tested in the 4–20 GHz frequency range. Tsitsas et al. [44] investigated periodic grating waveguides by using a rigorous integral equation method, which combined semi-analytical techniques and the Method of Moments with entire domain basis functions. In their work [44], they provided a showcase for the effect of the incident field's and grating's characteristics on the diffraction process, as well as the grating structure's efficient operation as a narrow-band reflection filter. In addition, Norton et al. [45] used the rigorous coupled-wave analysis method to provide physical insights into the factors contributing to filter bandwidth. Moreover, by the means of rigorous semi-analytical integral equation, Tsitsas [46] proposed a methodology that is characterized by high numerical stability and controllable accuracy. His obtained solution helped to investigate the operation of a metasurface as a narrow-band reflection frequency filter [46]. In this simulation work, we are not limited to the filtering of visible color, but we study the configuration of Fibonacci and Generalized Fibonacci structures

that allow the construction of high- and low-pass filters for the wavelengths (650, 850, 1300 and 1550 nm) of plastic and glass optical fibers.

2. Method and Problem Formulation

2.1. Transfer Matrix Method

In this numerical simulation, the transfer matrix method (TMM) is exercised to study optical wave propagation through periodic and quasi-periodic (Fibonacci and Generalized Fibonacci) photonic crystals. The transmittance T and the reflectance R of the wave are studied in this paper. Based on the TMM method, the amplitude of the input electric field E_0^+ , the reflected one E_0^- , and the output (transmitted) one E_{m+1}^+ after m layers are correlated using the following Equation [5]:

$$\begin{bmatrix} E_0^+ \\ E_0^- \end{bmatrix} = \prod_{j=1}^m C_j \begin{bmatrix} E_{m+1}^+ \\ E_{m+1}^- \end{bmatrix} \tag{1}$$

Here, C_j is the complex transfer matrix, and t_j is the transmittance Fresnel coefficient. The wave has two polarization modes (transverse electric (TE) and transverse magnetic (TM)).

For both polarization modes, the matrix C_j is expressed as follows [5]:

$$C_j = \begin{pmatrix} \exp(i\varphi_{j-1}) & r_j \exp(-i\varphi_{j-1}) \\ r_j \exp(i\varphi_{j-1}) & \exp(-i\varphi_{j-1}) \end{pmatrix} \tag{2}$$

Here, φ_{j-1} represents the phase shift of the wave between the j th/ $(j - 1)$ th layers (or boundaries) [5]:

$$\varphi_{j-1} = \frac{2\pi}{\lambda} \hat{n}_{j-1} d_{j-1} \cos \theta_{j-1} \tag{3}$$

In Equations (1) and (2), t_j and r_j represent the transmittance and reflectance Fresnel coefficients, respectively.

For TM (P-mode) polarization mode and TE (S-mode) mode, the Fresnel coefficients are expressed as follows [5]:

$$r_{jp} = \frac{\hat{n}_{j-1} \cos \theta_j - \hat{n}_j \cos \theta_{j-1}}{\hat{n}_{j-1} \cos \theta_j + \hat{n}_j \cos \theta_{j-1}} \tag{4}$$

$$t_{jp} = \frac{2\hat{n}_{j-1} \cos \theta_{j-1}}{\hat{n}_{j-1} \cos \theta_j + \hat{n}_j \cos \theta_{j-1}} \tag{5}$$

$$r_{js} = \frac{\hat{n}_{j-1} \cos \theta_{j-1} - \hat{n}_j \cos \theta_j}{\hat{n}_{j-1} \cos \theta_{j-1} + \hat{n}_j \cos \theta_j} \tag{6}$$

$$t_{js} = \frac{2\hat{n}_{j-1} \cos \theta_{j-1}}{\hat{n}_{j-1} \cos \theta_{j-1} + \hat{n}_j \cos \theta_j} \tag{7}$$

Here, \hat{n}_j and θ_j represent the complex refractive index of the materials and the complex refractive angle of the wave, respectively.

For both polarizations, the transmittance energies T are simplified as [5]

$$t_{js} = \frac{2\hat{n}_{j-1} \cos \theta_{j-1}}{\hat{n}_{j-1} \cos \theta_{j-1} + \hat{n}_j \cos \theta_j} \tag{8}$$

$$T_{rp} = \operatorname{Re} \left(\frac{\hat{n}_{m+1} \cos \theta_{m+1}}{\hat{n}_0 \cos \theta_0} \right) |t_p|^2 \tag{9}$$

2.2. Fibonacci and Generalized Fibonacci Quasi-Crystals Models

The Fibonacci multi-layer structure [7,13,27] can be built up using two different material layers, H and L. Here, the symbols H and L represent layers with a high (n_H) and low (n_L) refractive index, respectively. The geometric thicknesses of the H and L layers are d_H and d_L , respectively. The first two sequences of the Fibonacci model start with $S_0 = H$ and $S_1 = L$; then, using the substitution rule $L \rightarrow LH$ and $H \rightarrow L$, we can determine the next generations. The resulting 1D Fibonacci structure is quasi-periodic. For example, the sixth iteration has the form $S_6 = LHLLHLHLLHLLH$.

The interest in GF (m, n) quasi-periodic structures has increased since it appears that the physical properties of the Fibonacci sequence may not be genetic in some fundamental respects [1,2]. In addition, the Generalized Fibonacci (GF) (m, n) sequence [4,5,23] consists of two different layers (H and L). The starter sequences are $S_0 = H$ and $S_1 = L$, and, after that, the recursion relation of the GF (m, n) sequence is expressed as $S_{l+1} = S_l^m S_{l-1}^n$ for $l \geq 1$. Here, the parameters m and n represent the power (the successive repetition) of the sequence. For example, when $m = 2$ and $n = 1$, the recursive sequences will be $S_2 = LLH$, $S_3 = LLHLLH$, $S_4 = LLHLLHLLHLLHLLH$, etc. [4]. In addition, when $m = 1$ and $n = 2$, we obtain $S_2 = LHH$, $S_3 = LHHLL$, $S_4 = LHHLLHHLHH$, etc. The geometric photonic structure of this latest sequence ($S_4 = LHHLLHHLHH$) is illustrated as an example in Figure 1.

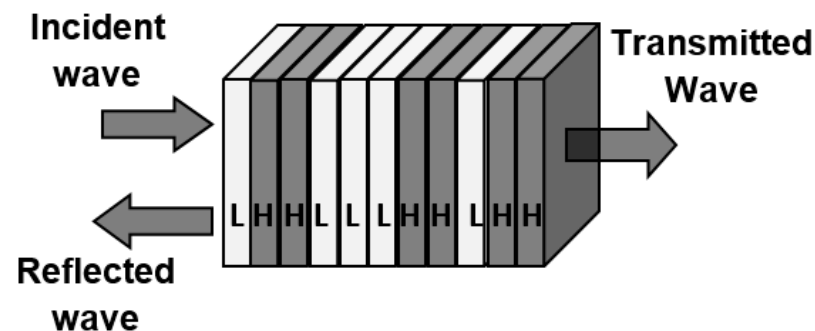


Figure 1. Schematic representation showing the geometry of the 4th generation of Generalized Fibonacci photonic GF (1, 2) structure.

3. Results and Discussion

In this work, we simulate the optical behavior of periodic, Fibonacci, and Generalized Fibonacci photonic structures. The materials that constitute the layers of the photonic structures are silicon dioxide (SiO_2 , $n_L = 1.45$) and titanium dioxide (TiO_2 , $n_H = 2.3$). These materials are chosen in view of their availability and low price in the global market compared to other semiconductor materials. In addition, the range of the refractive index between these two materials makes it possible to obtain broad PBGs. The thicknesses $d_{L,H}$ of the H and L layers satisfy the Bragg condition, $n_L d_L = n_H d_H = \lambda_0/4$, where $\lambda_0 = 1 \mu\text{m}$ represents the reference wavelength. For the proposed photonic structures, the optical transmittance properties are investigated in the visible frequency spectrum and for normal wave incidence. Figure 2 shows the transmittance spectra as a function of the frequency f_0 (THz) for the periodic, Fibonacci, and GF photonic structures. First, we fix the number of layers of the periodic structure to 34, and this number is chosen so that the PBG is clear and wide. To compare the transmittance spectra of the three photonic structures, the geometric thicknesses and the number of layers are nearly the same. For this, the number of layers (P) of the Fibonacci and the GF structures is chosen to be 34 and 31, respectively. Here, the iteration number of the Fibonacci and GF sequences is chosen to be 8 and 3, respectively. In addition, for the GF sequence, the parameters m and n are chosen to be 5 and 1, respectively. Here, the parameters m and n are chosen in such a way that the number of layers of all structures (periodic, Fibonacci and GF) is approximate. For the periodic

structure, Figure 2 shows the presence of one large photonic band gap (PBG) centered at the reference frequency ($f_0 = 299.22$ THz). The Fibonacci structure presents two symmetric PBGs at about f_0 , and they are in juxtaposition with that of the periodic structure. The GF (5, 1) structure has three pseudo-PBGs: one centered at f_0 and the other two symmetrical at about this frequency. Therefore, it is clear here that the Fibonacci structure permits two resonance peaks (two propagation modes) and two PBGs located inside and outside the PBG of the periodic structure to be obtained, respectively. This physical phenomenon is due to the chaotic dispersion (quasi-periodicity) of the layers of the Fibonacci structure. In addition, the GF sequence permits this disorder of layers to be amplified, which allows the presence of three pseudo-PBGs. The locations of these three bands appear as a merging of the periodic and the Fibonacci bands. Therefore, the GF structure permits the area of the PBGs to be enlarged and the number of the resonance peaks to be increased. This physical phenomenon is due to the parameters m and n of the GF ($S_{l+1} = S_l^m S_{l-1}^n$) sequence. The variation in these parameters permits the redundancy of the periodic subsequences (S_l^m and S_{l-1}^n), which allows the perturbation of wave propagation through the structure.

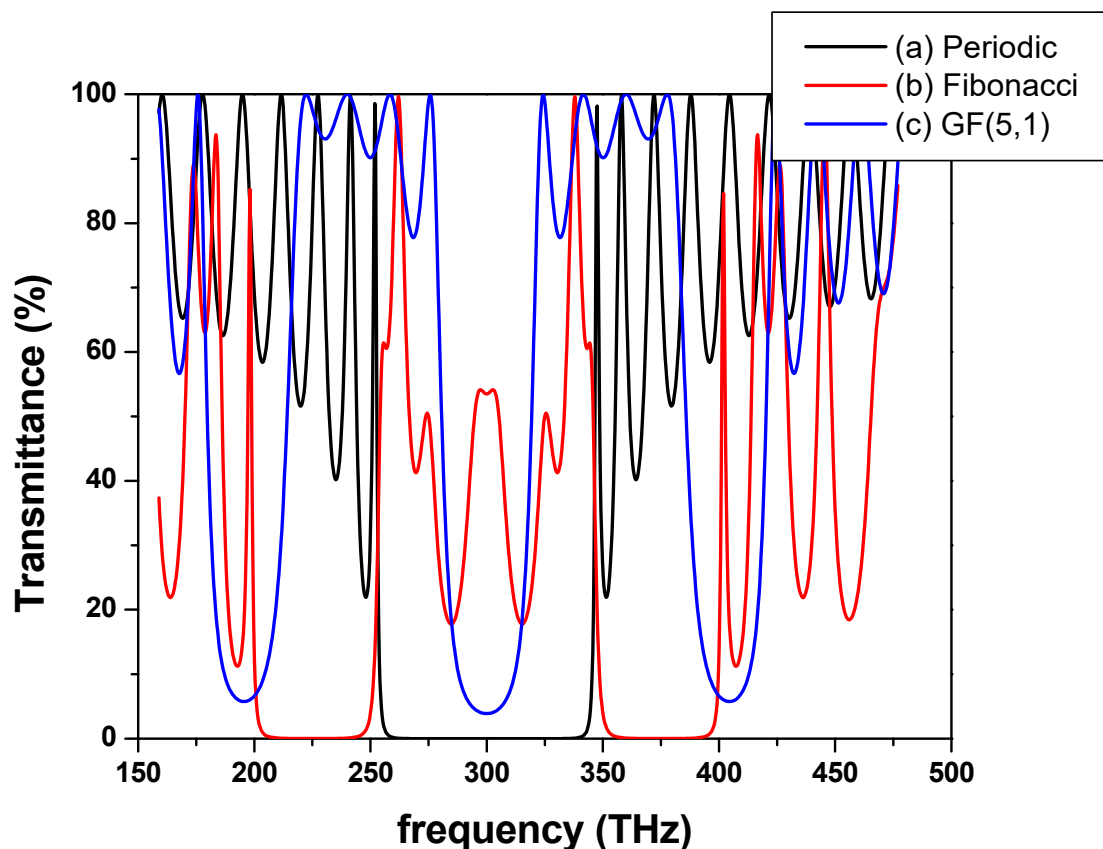


Figure 2. Transmittance spectra versus the frequency f (THz) for (a) periodic (34 layers, $d = 4.78 \mu\text{m}$), (b) Fibonacci (8th iteration, 34 layers, $d = 5.03 \mu\text{m}$), and (c) GF (5, 1) (3rd iteration, 31 layers, $d = 5.02 \mu\text{m}$).

Later and for the GF (m, n) sequence, the effect of varying the parameters m and n on the transmittance behavior is studied. We try to achieve tunable multi-band-stop filters using this structure. Figure 3a–d show the effect of varying the parameter m from 5 to 20. Here, the parameter n and the iteration number are fixed at 1 and 3, respectively. Figure 3a–d display the presence of consecutive PBGs separated with several resonance modes. Therefore, it is clear from this figure that the GF ($m, 1$) structure forms a selective band-stop filter. In addition, we can notice that the number, the position, and the width of these PBGs depend on the parameter m of the GF ($m, 1$) structure.

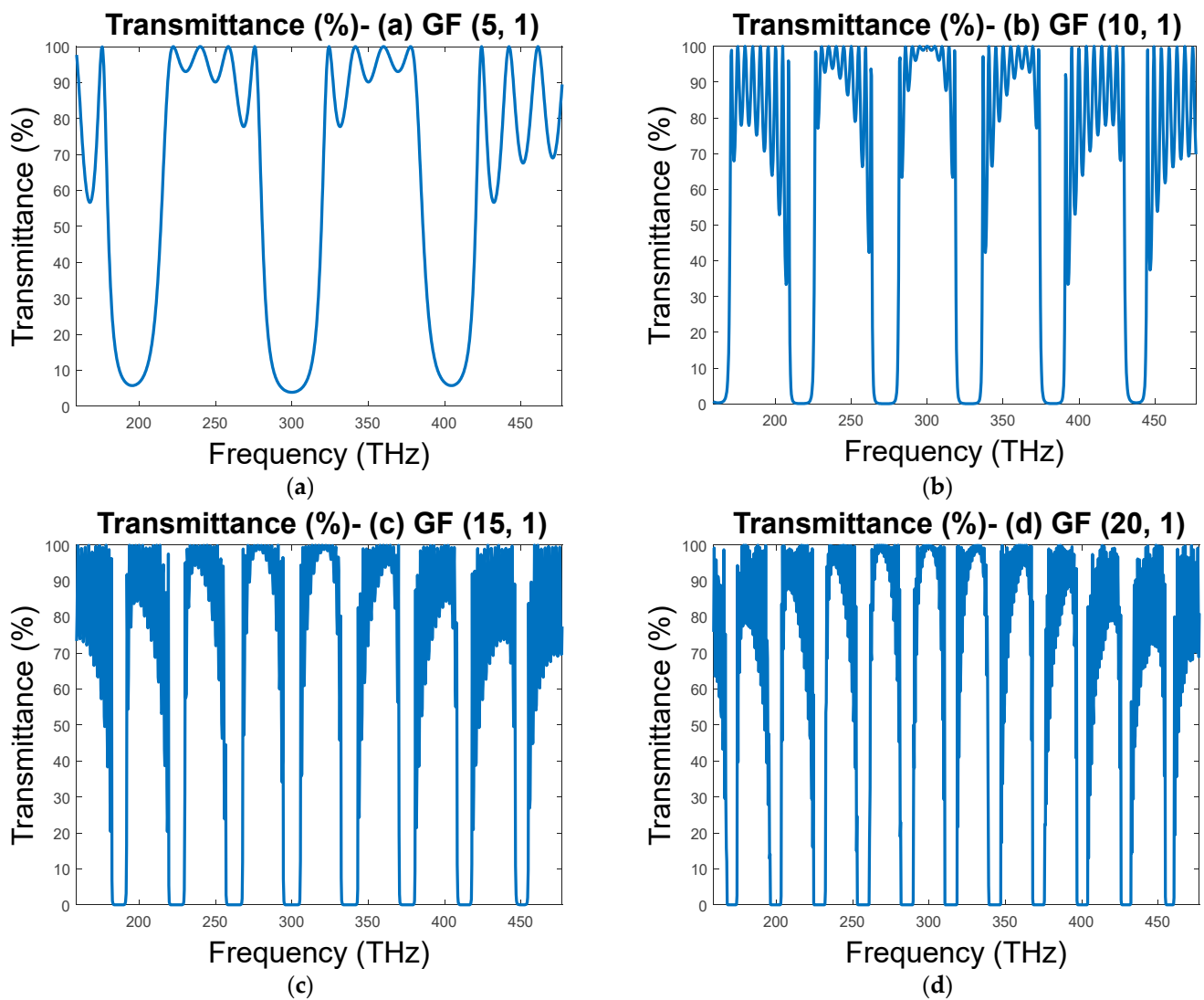


Figure 3. Transmittance spectra versus frequency for 1D GF sequence (3rd iteration) and for (a) GF (5, 1), (b) GF (10, 1), (c) GF (15, 1), and (d) GF (20, 1).

Figure 4 shows the relationship between the number of PBGs and the parameter m . It is clear that this dependence is linear, and the regression fit of this graph is $\text{NPBGs} = 0.5 + 0.52 \times m$, where the parameter NPBGs represent the number of PBGs. The pattern of data and the trend line in Figure 4 are indicative of the type of correlation between the two variables (NPBGs and m). Therefore, it is clear that the correlation is positive and strong. In addition, the Pearson correlation factor represents a statistic parameter showing the degree of relation between these two variables. In fact, the Pearson factor measures the nature and the strength between any two variables of the quantitative type. Using the data in Figure 4 and statistical software, we found that the Pearson factor between the parameter m and the number of NPBGs is equal to 0.997, so this correlation is positive and strong. Therefore, by adjusting the parameter m of the GF ($m, 1$) structure, we can tune the number, the position, and the width of these PBGs.

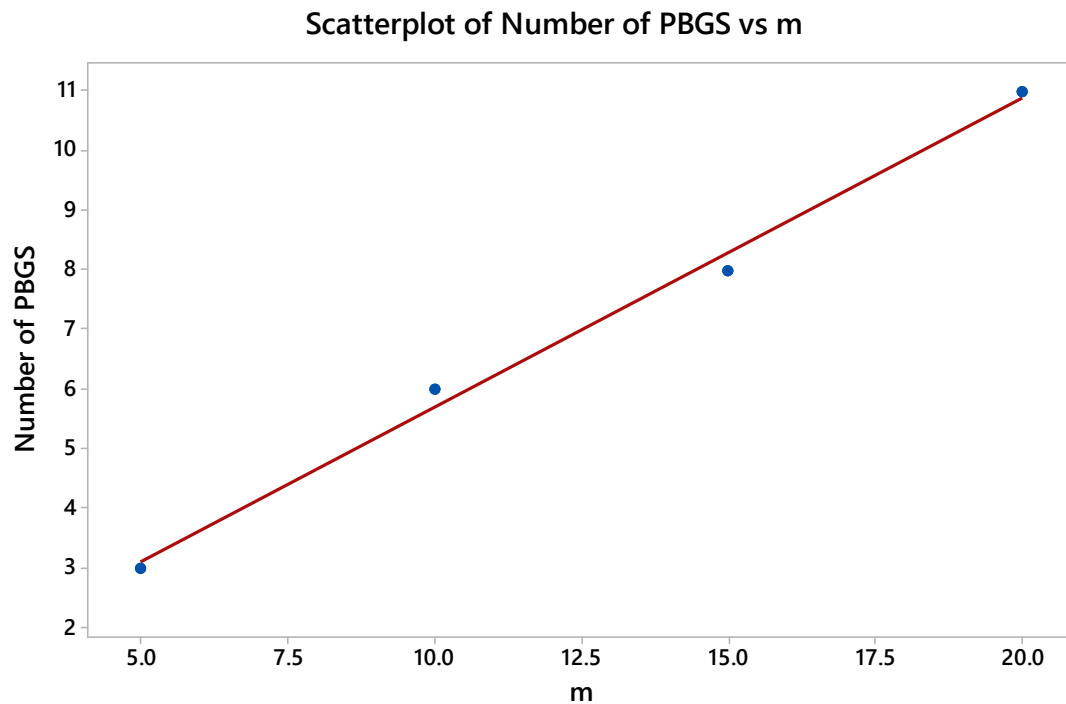


Figure 4. Number of PBGS as a function of the parameter m for 1D GF ($m, 1$) sequence (3^{rd} iteration).

The optical communication wavelengths used by the different types of optical fibers (plastic and glass optical fibers) are 650, 850, 1300, and 1550 nm, which correspond to the frequencies 461, 352.69, 230.46, and 193.37 THz, respectively. Table 1 shows the percentages of transmittance for these optical communication wavelengths with different GF ($m, 1$) photonic structures. The green cells represent the maximum percentage of transmittance for a given wavelength. For instance, the 650 nm wavelength fully passes ($T = 100\%$) through the GF (5, 1) structure, and the 1550 nm wavelength is reflected by the same structure. The GF (10, 1) structure is suitable to allow the 1300 nm wavelength of the multi-mode graded-index fiber to pass through. At the same time, the last wavelength is forbidden from transmitting by the GF (20, 1) structure. Table 1 demonstrates the possibility of using these tunable GF multi-band-stop filters in optical communication applications.

Table 1. Transmittance (%) for optical fiber wavelengths using the 3^{rd} iteration of GF ($m, 1$) structures.

Structures	Optical Fiber Wavelengths			
	650 nm	850 nm	1300 nm	1550 nm
GF (5, 1)	100	92.0	93	6
GF (10, 1)	70	87.0	100	75
F (15, 1)	96	96.0	64	90
GF (20, 1)	26	77.8	0	55

Figure 5a–d show the effect of the parameter n of the GF (1, n) structure on the transmittance spectra. This figure only displays the presence of the Kiessig fringes, and no PBG appears. This physical phenomenon is due to the distribution of layers; for example, for the GF (1, 5) structure, the distribution of layers is LHHHHHLLLLL. This structure works as though it is made by concentrating two successive thick H/L layers. Thus, there is no chaotic distribution of the H and L layers, which decreases the amount of reflection between the different layer interfaces. Therefore, the role of the transfer matrix is approximately negligible in the transmittance computation, and only the propagation matrix, through the same kind of layers, has a great effect on this computation.

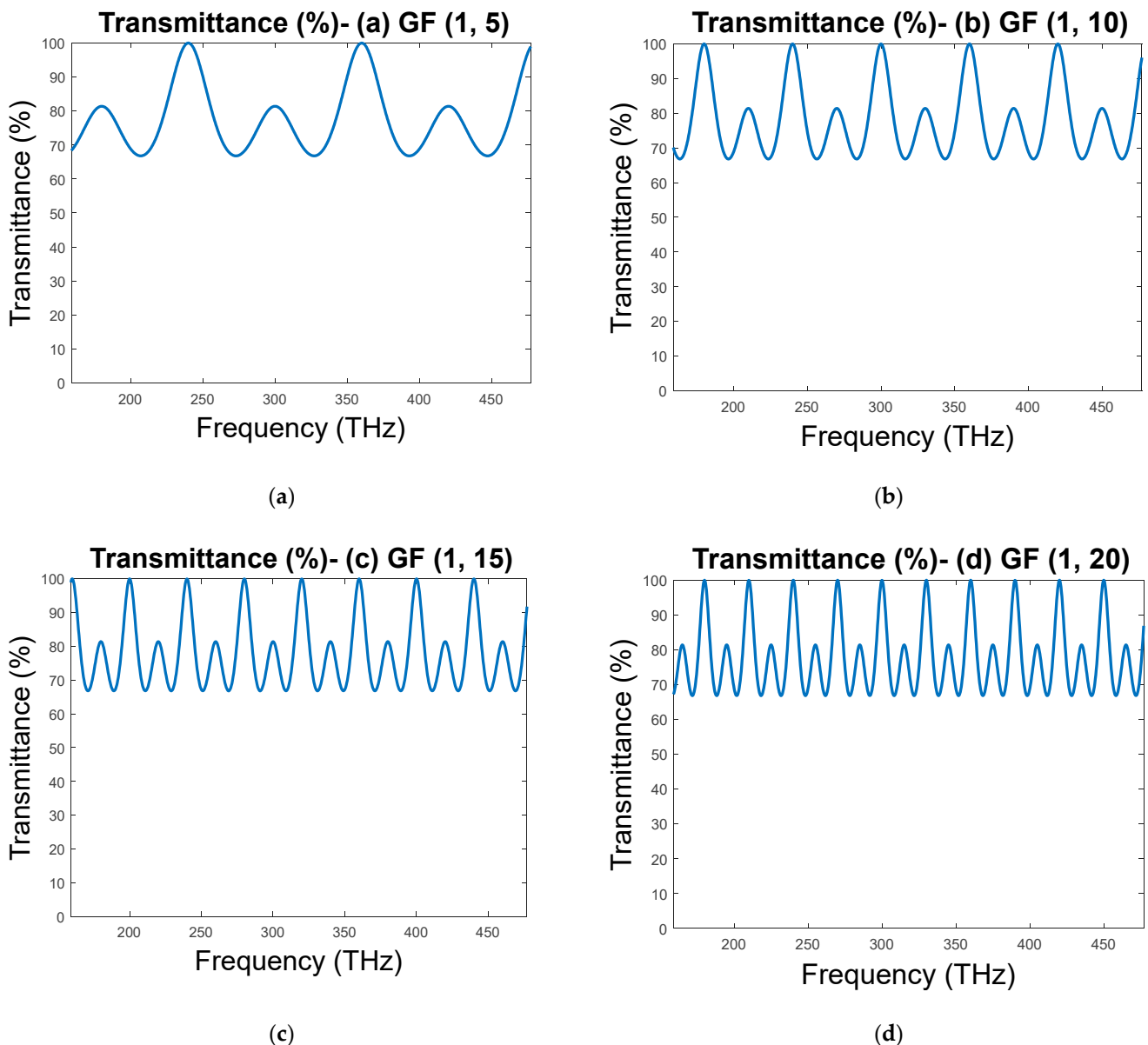


Figure 5. Transmittance spectra versus frequency for 1D GF sequence (3rd iteration) and for (a) GF (1, 5), (b) GF (1, 10), (c) GF (1, 15), and (d) GF (1, 20).

4. Conclusions

The numerical investigation of the Generalized Fibonacci (GF) (m, n) structures in this study permits us to conclude that only the parameter m permits the number, the position, and the width of several successive PBGs to be determined. The correlation between the parameter m and the number of PBGs is positive and strong (the Pearson correlation factor is 0.997). These phenomena permit us to consider the GF ($m, 1$) structure as tunable multi-band-stop filters for the optical telecommunication wavelengths of 650, 850, 1300 and 1550 nm. In fact, by varying the parameter m , we can allow the transmission of a given optical fiber wavelength and forbid others. In contrast, the variation in the parameter n for the GF ($1, n$) structures permits only several Kiessig fringes to be obtained, without noticing any PBGs, and this physical phenomenon is due to the distribution of two material layers when only two successive blocks of H and L layers are found.

Author Contributions: Conceptualization, N.B.A. and Y.T.; methodology, H.A.; software, N.B.A. and Z.E.; validation, N.B.A. and S.A.; formal analysis, N.B.A.; investigation, S.A.; resources, H.A.; data curation, N.B.A. and O.K.; writing—original draft preparation, N.B.A. and Y.T.; writing—review and editing, N.B.A. and O.K.; visualization, Z.E.; supervision, N.B.A.; project administration, N.B.A.; funding acquisition, all authors. All authors have read and agreed to the published version of the manuscript.

Funding: This research was funded by the Scientific Research Deanship at the University of Ha'il—Saudi Arabia through project number RG-21 077.

Institutional Review Board Statement: Not applicable.

Informed Consent Statement: Not applicable.

Data Availability Statement: Not applicable.

Conflicts of Interest: The authors declare no conflict of interest.

References

1. Augustyniak, A.; Zdanowicz, M.; Osuch, T. Self-Similarity Properties of Complex Quasi-Periodic Fibonacci and Cantor Photonic Crystals. *Photonics* **2021**, *8*, 558. [[CrossRef](#)]
2. Kohmoto, M.; Sutherland, B.; Iguchi, K. Localization in Optics: Quasiperiodic Media. *Phys. Rev. Lett.* **1987**, *58*, 2436. [[CrossRef](#)] [[PubMed](#)]
3. Ali, N.B.; Zaghdoudi, J.; Kanzari, M.; Kuszelewicz, R. The slowing of light in one-dimensional hybrid periodic and non-periodic photonic crystals. *J. Opt.* **2010**, *12*, 045402. [[CrossRef](#)]
4. Trabelsi, Y.; Ali, N.B.; Segovia-Chaves, F.; Posada, H.V. Photonic band gap properties of one-dimensional photonic quasicrystals containing Nematic liquid crystals. *Results Phys.* **2020**, *19*, 103600. [[CrossRef](#)]
5. Ali, N.B.; Trabelsi, Y.; Kanzari, M. Stop band filter by using hybrid quasi-periodic one dimensional photonic crystal in microwave domain. *IJMOT* **2009**, *4*, 195–204.
6. Ali, N.B.; Dhasarathan, V.; Alsaif, H.; Trabelsi, Y.; Nguyen, T.; Bouazzi, Y.; Kanzari, M. Design of output-graded narrow polychromatic filter by using photonic quasicrystals. *Phys. B Condens. Matter* **2020**, *582*, 411918. [[CrossRef](#)]
7. Ali, N.B.; Kanzari, M. omni-directional high reflectors using one-dimensional deformed quasi-periodic Cantor band gap structure at optical telecommunication wavelength band. *Mediterr. J. Electron. Commun.* **2010**, *6*, 1–6.
8. Segovia-Chaves, F.; Posada, H.V.; Trabelsi, Y.; Ali, N.B. Transmittance spectrum in a one-dimensional photonic crystal with Fibonacci sequence superconductor–semiconductor. *Optik* **2020**, *217*, 164803. [[CrossRef](#)]
9. Han, P.; Wang, H.Z. Effect of invariant transformation in one-dimensional randomly-perturbed photonic crystal. *Chin. Phys. Lett.* **2003**, *20*, 1520.
10. Merlin, R.; Bajema, K.; Clarke, R.; Juang, F.Y.; Bhattacharya, P.K. Quasiperiodic GaAs-AlAs heterostructures. *Phys. Rev. Lett.* **1985**, *55*, 1768. [[CrossRef](#)]
11. Kohmoto, M.; Sutherland, B. Critical wave functions and a Cantor-set spectrum of a one-dimensional quasicrystal model. *Phys. Rev. B* **1987**, *35*, 1020. [[CrossRef](#)] [[PubMed](#)]
12. Sibilia, C.; Bertolotti, M. Trends in Optics and Photonics. In *ICO Book IV Trends in Optics and Photonics*; Asakura, T., Ed.; Springer: New York, NY, USA, 1999.
13. Chakrabarti, A. Field induced delocalization in a Koch fractal. *Phys. Rev. B* **1999**, *60*, 10576–10579. [[CrossRef](#)]
14. Gellermann, W.; Kohmoto, M.; Sutherland, B.; Taylor, P.C. Localization of light waves in Fibonacci dielectric multilayers. *Phys. Rev. Lett.* **1994**, *72*, 633–636. [[CrossRef](#)] [[PubMed](#)]
15. Barry, G.G.; Howard, H.; Ramzi, H.N. Optical processors for smart structures. In Proceedings of the Advances in Optical Information Processing IV, Orlando, FL, USA, 1 September 1990; Volume 1296. [[CrossRef](#)]
16. Luo, D.; Hao, Q. Optical transmission link between microprocessors and memories. In Proceedings of the Asia Communications and Photonics Conference, Shanghai, China, 11–14 November 2014; ISBN 978-1-55752-852-0. [[CrossRef](#)]
17. Alexoudi, T.; Kanellos, G.T.; Pleros, N. Optical RAM and integrated optical memories: A survey. *Light Sci. Appl.* **2020**, *9*, 91. [[CrossRef](#)]
18. Leonardo, D.B.; Niall, M.; Pascal, D. Optical memories and switching dynamics of counterpropagating light states in microresonators. *Opt. Express* **2021**, *29*, 2193–2203. [[CrossRef](#)]
19. Heim, B.; Soeken, M.; Marshall, S.; Granade, C.; Roetteler, M.; Geller, A.; Troyer, M.; Svore, K. Quantum programming languages. *Nat. Rev. Phys.* **2020**, *2*, 709–722. [[CrossRef](#)]
20. LeeAnn, M.S.; Scott, E.S.; David, A.M. Preparation of an exciton condensate of photons on a 53-qubit quantum computer. *Phys. Rev. Res.* **2020**, *2*, 043205. [[CrossRef](#)]
21. Jin, C.J.; Cheng, B.Y.; Man, B.Y.; Li, Z.L.; Zhang, D.Z. Two-dimensional dodecagonal and decagonal quasiperiodic photonic crystals in the microwave region. *Phys. Rev. B* **2000**, *61*, 10762–10767. [[CrossRef](#)]

22. Trabelsi, Y.; Ali, N.B.; Segovia-Chaves, F.; Posada, H.V. Tunable 1D nano-photonic filter using Nematic liquid crystal and high-Tc superconductors. *Opt. Quant. Electron.* **2021**, *53*, 712. [[CrossRef](#)]
23. Huang, X.Q.; Jiang, S.S.; Peng, R.W.; Hu, A. Perfect transmission and self-similar optical transmission spectra in symmetric Fibonacci-class multilayers. *J. Phys. Rev. E* **2001**, *59*, 245104. [[CrossRef](#)]
24. Belhadj, W.; Ali, N.B.; Dakhlaoui, H.; Alsalmi, O.H.; Alsaif, H.; Torchani, A. Characterization of spectral features of cavity modes in one-dimensional graphene-based photonic crystal structures, *Eur. Phys. J. B* **2021**, *94*, 198. [[CrossRef](#)]
25. Trabelsi, Y.; Ben Ali, N.; Belhadj, W.; Kanzari, M. Photonic Band Gap Properties of One-dimensional Generalized Fibonacci Photonic Quasicrystal Containing Superconductor Material. *J. Supercond. Nov. Magn.* **2019**, *32*, 3541–3547. [[CrossRef](#)]
26. Gahef, T.; Bouazzi, Y.; Kanzari, M. Omnidirectional mirror at 1.3 and 1.55 μm for optical fiber communication by specific deformation of Bragg reflector. *Opt. Quant. Electron.* **2017**, *49*, 95. [[CrossRef](#)]
27. Chittaranjan, N.; Alireza, A.; Ardendu, S.; Narottam, D. Near- and mid-infrared bandgaps in a 1D photonic crystal containing superconductor and semiconductor-metamaterial. *Int. J. Mod. Phys. B* **2019**, *33*, 1950219. [[CrossRef](#)]
28. Augusto, D.A.F.; Luis, M.G.S.; Vivechana, A. Study of the omnidirectional photonic bandgap for dielectric mirrors based on porous silicon: Effect of optical and physical thickness. *Nanoscale Res. Lett.* **2012**, *7*, 391. [[CrossRef](#)]
29. Ali, N.B.; Kanzari, M. Designing of omni-directional high reflectors by using one-dimensional modified hybrid Fibonacci/Cantor band-gap structures at optical telecommunication wavelength band. *J. Mod. Opt.* **2010**, *57*, 287–294. [[CrossRef](#)]
30. Sanjeev, S.; Rajender, K.; Singh, K.S.; Kumar, V.; Deepti, J. Design of a Narrow-Band Photonic Crystal Based Omni-Directional Mirror for Optical Fiber Communication. *IJECSE* **2012**, *1*, 1825–1832.
31. Ali, N.B.; Trabelsi, Y.; Alsaif, H.; Badawi, I.; Gal, S. Omnidirectional High Reflectors Using Silica/Superconductor Fibonacci Photonic Crystal for Optical Communication Applications. *Phys. C: Supercond. Its Appl.* **2022**, *594*, 1354021. [[CrossRef](#)]
32. Ahmad, I.; Ullah, S.; Ullah, S.; Habib, U.; Ahmad, S.; Ghaffar, A.; Alibakhshikenari, M.; Khan, S.; Limiti, E. Design and Analysis of a Photonic Crystal Based Planar Antenna for THz Applications. *Electronics* **2021**, *10*, 1941. [[CrossRef](#)]
33. Mao, H.; Lu, G. Enhancement of THz Photoconductive Antenna Gain based on a Photonic Crystal Fiber Substrate. In Proceedings of the IEEE International Symposium on Antennas and Propagation and USNC-URSI Radio Science Meeting (APS/URSI), Singapore, 16 February 2022. [[CrossRef](#)]
34. Geler-Kremer, J.; Eltes, F.; Stark, P.; Sharma, A.; Caimi, D.; Offrein, B.J.; Fompeyrine, J.; Abel, S. A Non-Volatile Optical Memory in Silicon Photonics. In Proceedings of the Optical Fiber Communications Conference and Exhibition (OFC) IEEE, San Francisco, CA, USA, 6–10 June 2021.
35. Mohammadi, M.; Farahmand, M.; Olyaei, S.; Seifouri, M. An Overview of All-Optical Memories Based on Periodic Structures Used in Integrated Optical Circuits. *Silicon* **2022**, *14*, 54. [[CrossRef](#)]
36. Bartlett, B.; Dutt, A.; Fan, S. Deterministic photonic quantum computation in a synthetic time dimension. *Optica* **2021**, *8*, 1515–1523. [[CrossRef](#)]
37. Ochoa, M.; Algorri, J.F.; Roldán-Varona, P.; Rodríguez-Cobo, L.; López-Higuera, J.M. Recent Advances in Biomedical Photonic Sensors: A Focus on Optical-Fibre-Based Sensing. *Sensors* **2021**, *21*, 6469. [[CrossRef](#)] [[PubMed](#)]
38. Ali, N.B.; Alsaif, H.; Trabelsi, Y.; Chughtai, M.T.; Dhasarathan, V.; Kanzari, M. High Sensitivity to Salinity-Temperature Using One-Dimensional Deformed Photonic Crystal. *Coatings* **2021**, *11*, 713. [[CrossRef](#)]
39. Yu, B.; Luo, Y.; Chen, L.; Chu, Z.; Li, K.H. An optical humidity sensor: A compact photonic chip integrated with artificial opal. *Sens. Actuators B Chem.* **2021**, *349*, 130763. [[CrossRef](#)]
40. Lio, G.E.; Ferraro, A. LIDAR and Beam Steering Tailored by Neuromorphic Metasurfaces Dipped in a Tunable Surrounding Medium. *Photonics* **2021**, *8*, 65. [[CrossRef](#)]
41. Shaltout, A.M.; Kim, J.; Boltasseva, A.; Shalaev, V.M.; Kildishev, A.V. Ultrathin and multicolour optical cavities with embedded metasurfaces. *Nat. Commun.* **2018**, *9*, 2673. [[CrossRef](#)]
42. Lio, G.E.; Ferraro, A.; Giocondo, M.; Caputo, R.; De Luca, A. Color Gamut Behavior in Epsilon Near-Zero Nanocavities during Propagation of Gap Surface Plasmons. *Adv. Opt. Mater.* **2020**, *8*, 2000487. [[CrossRef](#)]
43. Tibuleac, S.; Magnusson, R.; Maldonado, T.A.; Young, P.P.; Holzheimer, T.R. Dielectric frequency-selective structures incorporating waveguide gratings. *IEEE Trans. Microw. Theory Tech.* **2000**, *48*, 553–561. [[CrossRef](#)]
44. Tsitsas, N.L.; Uzunoglu, N.K.; Kaklamani, D.I. Diffraction of plane waves incident on a grating dielectric slab: An entire domain integral equation analysis. *Radio Sci.* **2007**, *42*, RS6S22. [[CrossRef](#)]
45. Norton, S.M.; Turan, E.; Michael, G.M. Coupled-mode theory of resonant-grating filters. *J. Opt. Soc. Am. A* **1997**, *14*, 629–639. [[CrossRef](#)]
46. Tsitsas, N.L. Efficient integral equation modeling of scattering by a gradient dielectric metasurface. *EPJ Appl. Metamater.* **2017**, *43*, 3. [[CrossRef](#)]